



$M1$ resonance in ^{208}Pb within the self-consistent phonon-coupling modelV. Tselyaev * and N. Lyutorovich *St. Petersburg State University, St. Petersburg, 199034, Russia*J. Speth *Institut für Kernphysik, Forschungszentrum Jülich, D-52425 Jülich, Germany*P.-G. Reinhard *Institut für Theoretische Physik II, Universität Erlangen-Nürnberg, D-91058 Erlangen, Germany*

(Received 12 October 2020; revised 18 November 2020; accepted 7 December 2020; published 23 December 2020)

The main goal of the paper is to investigate the experimentally observed spectral fragmentation of the isovector $M1$ resonance in ^{208}Pb within a self-consistent model based on an energy-density functional (EDF) of the Skyrme type. This fragmentation is not reproduced in a conventional one-particle–one-hole (1p1h) random-phase approximation (RPA) and thus has to be investigated in the framework of models including complex configurations. However, previously applied models of this type were not self-consistent. In the present work, we use a recently developed renormalized version of the self-consistent time-blocking approximation (RenTBA) in which 1p1h \otimes phonon configurations are included on top of the RPA 1p1h configurations. We have investigated several parameter sets of modified Skyrme EDFs which were fitted within the RenTBA and RPA to reproduce the basic experimental characteristics of the low-energy $M1$ excitations in ^{208}Pb . We have found as a necessary condition for producing the appropriate fragmentation of the $M1$ resonance in ^{208}Pb that the minimum energy of the intermediate 1p1h \otimes phonon configurations comes close to the mean energy of the $M1$ resonance. We present also results of the RenTBA and RPA calculations for the first excited states of the natural parity modes in ^{208}Pb obtained with the modified parametrizations.

DOI: [10.1103/PhysRevC.102.064319](https://doi.org/10.1103/PhysRevC.102.064319)**I. INTRODUCTION**

Magnetic dipole ($M1$) excitations in the ^{208}Pb nucleus were the object of numerous experimental and theoretical investigations for several decades. From the theoretical point of view, this mode is interesting because it allows to determine the spin-related parameters of the residual interaction within the random-phase approximation (RPA) or its extended versions. In the self-consistent approach, the residual interaction is defined by an energy-density functional (EDF), in particular, by the EDF of Skyrme type [1]. The calculated energies of the unnatural parity excitations in such an approach are very sensitive to the values of the spin-related parameters of the EDF. Therefore, the comparison of $M1$ spectra with experimental data helps enormously to confine the EDF parameters of this type. Another crucial aspect is the fragmentation (spread) of the isovector $M1$ resonance in ^{208}Pb which is observed in the experiment (see [2]) but which is absent in RPA where the isovector $M1$ strength in this nucleus is concentrated in one state. The description of this fragmentation requires application of more complicated models going beyond the RPA framework (see, e.g., Ref. [3] for more details).

Most of the early calculations of the $M1$ excitations in ^{208}Pb (see, e.g., Refs. [4–8]) were performed within the RPA, the Tamm-Dancoff approximation or within the Migdal's Theory of Finite Fermi Systems (TFFS, Ref. [9]) which in its simplest form, as used in the applications, is equivalent to RPA with a zero-range residual interaction. Later on, the $M1$ modes were investigated within the generalized models in which the one-particle–one-hole (1p1h) RPA configuration space is enlarged by adding 2p2h, 1p1h \otimes phonon or two-phonons configurations (see, e.g., Refs. [10–18]). However, fully self-consistent calculations of the $M1$ excitations in ^{208}Pb have been performed so far only within RPA (see Refs. [19–24]).

In a broad sense, self-consistency means the use of the same EDF $E[\rho]$ (where ρ is the single-particle density matrix) for the mean field as well as for the RPA residual interaction. This reduces the number of the free parameters of the theory and, in turn, increases its predictive power. Here we use an EDF of Skyrme type [1]. In a recent paper [24], we have shown that the adequate description of the low-energy $M1$ excitations in ^{208}Pb within the self-consistent RPA based on the Skyrme EDF is possible only if the spin-related parameters of the known EDF are modified. By re-tuning these parameters, we managed to reproduce within RPA the experimental key quantities: energy and strength of the 1_1^+ state as well as mean energy and summed strength of the $M1$ resonance in ^{208}Pb in the interval 6.6–8.1 MeV. However, as mentioned above, the

*tselyaev@mail.ru

observed fragmentation of the isovector $M1$ resonance and its total width are not reproduced in this model.

The aim of the present paper is to study how one could possibly describe this fragmentation within an extended self-consistent model including $1p1h \otimes$ phonon configurations on top of the RPA $1p1h$ configurations. This extended model is treated within the time blocking approximation (TBA) which we use actually in its renormalized version (RenTBA, [25]). Full self-consistency is maintained also for the extended treatment. The method of re-tuning the spin-related parameters of the Skyrme EDF developed in Ref. [24] is used also for the RenTBA.

The paper is organized as follows. In Sec. II, the formalism of RPA and RenTBA is briefly described. Section III contains the numerical details and the calculation scheme. The main results of the paper are presented in Sec. IV. In Sec. V, the fine structure of the $M1$ strength distributions in ^{208}Pb and the impact of the single-particle continuum on this structure are analyzed. In Sec. VI, the problem of the fragmentation of the isovector $M1$ resonance in ^{208}Pb is discussed in detail and the necessary condition of the description of this fragmentation is worked out. In Sec. VII, we present the results of the RenTBA and RPA calculations of the low-energy electric excitations in ^{208}Pb obtained with the modified parametrizations of the Skyrme EDF. Conclusions are given in the last section.

II. THE MODEL

Let us start with the RPA eigenvalue equation

$$\sum_{34} \Omega_{12,34}^{\text{RPA}} Z_{34}^n = \omega_n Z_{12}^n, \quad (1)$$

where ω_n is the excitation energy, Z_{12}^n is the transition amplitude, and the numerical indices (1, 2, 3, ...) stand for the sets of the quantum numbers of the given single-particle basis. In what follows the indices p and h are used to label the states of the particles and holes in the basis which diagonalizes the single-particle density matrix ρ and the single-particle Hamiltonian h in the ground state [see Eq. (5) below]. The transition amplitudes are normalized by the condition

$$\langle Z^n | M^{\text{RPA}} | Z^n \rangle = \text{sgn}(\omega_n), \quad (2)$$

where

$$M_{12,34}^{\text{RPA}} = \delta_{13} \rho_{42} - \rho_{13} \delta_{42} \quad (3)$$

is the metric matrix in the RPA.

In the self-consistent RPA based on the EDF $E[\rho]$, the RPA matrix Ω^{RPA} is defined by

$$\Omega_{12,34}^{\text{RPA}} = h_{13} \delta_{42} - \delta_{13} h_{42} + \sum_{56} M_{12,56}^{\text{RPA}} V_{56,34}, \quad (4)$$

where the single-particle Hamiltonian h and the amplitude of the residual interaction V are linked by the relations

$$h_{12} = \frac{\delta E[\rho]}{\delta \rho_{21}}, \quad V_{12,34} = \frac{\delta^2 E[\rho]}{\delta \rho_{21} \delta \rho_{34}}. \quad (5)$$

In the TBA, the counterpart of Eq. (1) has the form

$$\sum_{34} \Omega_{12,34}^{\text{TBA}}(\omega_\nu) z_{34}^\nu = \omega_\nu z_{12}^\nu, \quad (6)$$

where

$$\Omega_{12,34}^{\text{TBA}}(\omega) = \Omega_{12,34}^{\text{RPA}} + \sum_{56} M_{12,56}^{\text{RPA}} \bar{W}_{56,34}(\omega), \quad (7a)$$

$$\bar{W}_{12,34}(\omega) = W_{12,34}(\omega) - W_{12,34}(0). \quad (7b)$$

The matrix $\Omega^{\text{TBA}}(\omega)$ is energy-dependent because the matrix of the induced interaction $W(\omega)$ depends on energy through the intermediate $1p1h \otimes$ phonon configurations. The subtraction of $W(0)$ in Eq. (7b) serves to maintain the mean-field ground state [26,27] and to ensure stability of solutions of the TBA eigenvalue equation (see Ref. [28]). The matrix $W(\omega)$ is defined by the equations

$$W_{12,34}(\omega) = \sum_{c, \sigma} \frac{\sigma F_{12}^{c(\sigma)} F_{34}^{c(\sigma)*}}{\omega - \sigma \Omega_c}, \quad (8a)$$

$$\Omega_c = \varepsilon_{p'} - \varepsilon_{h'} + \omega_\nu, \quad \omega_\nu > 0, \quad (8b)$$

where $\sigma = \pm 1$, $c = \{p', h', \nu\}$ is a combined index for the $1p1h \otimes$ phonon configurations, ν is the phonon's index, $\varepsilon_{p'}$ and $\varepsilon_{h'}$ are the particle's and hole's energies, and ω_ν is the phonon's energy. The amplitudes $F_{12}^{c(\sigma)}$ have only particle-hole matrix elements $F_{ph}^{c(\sigma)}$ and $F_{hp}^{c(\sigma)}$. They are defined by the equations

$$F_{12}^{c(-)} = F_{21}^{c(+)*}, \quad F_{ph}^{c(-)} = F_{hp}^{c(+)} = 0, \quad (9a)$$

$$F_{ph}^{c(+)} = \delta_{pp'} g_{h'h}^\nu - \delta_{h'h} g_{pp'}^\nu, \quad (9b)$$

where g_{12}^ν is an amplitude of the particle-phonon interaction.

In the conventional TBA, the phonon's energies ω_ν in Eq. (8b) and the amplitudes g_{12}^ν in Eq. (9b) are determined within RPA. The nonlinear version of the TBA developed in Ref. [25] aims at a higher level of self-consistency in that the phonon's energies ω_ν are the solutions of the TBA Eq. (6), while the amplitudes g_{12}^ν are expressed through the transition amplitudes z_{12}^ν which are also the solutions of Eq. (6), namely,

$$g_{12}^\nu = \sum_{34} V_{12,34} z_{34}^\nu. \quad (10)$$

The normalization condition for the transition amplitudes z_{12}^ν has the form

$$(z^\nu)_{\text{RPA}}^2 + (z^\nu)_{\text{CC}}^2 = 1, \quad (11)$$

where

$$(z^\nu)_{\text{RPA}}^2 = \text{sgn}(\omega_\nu) \langle z^\nu | M^{\text{RPA}} | z^\nu \rangle, \quad (12a)$$

$$(z^\nu)_{\text{CC}}^2 = -\text{sgn}(\omega_\nu) \langle z^\nu | W'_\nu | z^\nu \rangle, \quad (12b)$$

$$W'_\nu = \left(\frac{dW(\omega)}{d\omega} \right)_{\omega=\omega_\nu}. \quad (12c)$$

The terms $(z^\nu)_{\text{RPA}}^2$ and $(z^\nu)_{\text{CC}}^2$ represent the contributions of the $1p1h$ components (RPA) and of the complex configurations (CC) to the norm Eq. (11). The model includes only

those TBA phonons that satisfy the condition

$$(z^\nu)_{\text{RPA}}^2 > (z^\nu)_{\text{CC}}^2, \quad (13)$$

which together with Eq. (11) means that

$$(z^\nu)_{\text{RPA}}^2 > \frac{1}{2}. \quad (14)$$

The condition Eq. (13) confines the phonon space to the RPA-like phonons in agreement with the basic model approximations.

The feedback described above renders the phonon space of TBA fully self-consistent. In the present paper we use the version of this nonlinear model in which the TBA energies ω_ν and the amplitudes z_{12}^ν entering Eqs. (8b) and (10) (and only in these equations) are determined from the solutions of the TBA Eq. (6) in the diagonal approximation. In this approximation we have: $|z^\nu\rangle = \zeta_{n,q} |Z^n\rangle$, where $\nu = (n, q)$, q is the index of the fragmented RPA state, $|Z^n\rangle$ is the RPA transition amplitude, and $\zeta_{n,q}$ is the renormalization factor [with $\zeta_{n,q}^2 > 1/2$ for the phonons satisfying the condition Eq. (14)]. This model is what we call the renormalized TBA (RenTBA, see Ref. [25] for more details).

III. NUMERICAL DETAILS AND THE CALCULATION SCHEME

The equations of RPA and RenTBA were solved within the fully self-consistent scheme as described in Refs. [29–31]. Wave functions and fields were represented on a spherical grid in coordinate space. The single-particle basis was discretized by imposing box boundary condition with a box radius of 18 fm. The single particle energies ε_p were limited by the maximum value $\varepsilon_p^{\text{max}} = 100$ MeV. The nonlinear RenTBA equations were solved by an iterative procedure. The phonon space of the first iteration started from the RPA phonons with the energies $\omega_n \leq 50$ MeV and multipolarities $L \leq 15$ of both the electric and magnetic types which have been selected according to the criterion of collectivity

$$\langle Z^n | V^2 | Z^n \rangle / \omega_n^2 \geq 0.05, \quad (15)$$

see Ref. [25].

The field operator \mathcal{Q} in the case of the $M1$ excitations was taken in the form (see, e.g., Refs. [9,32])

$$\mathcal{Q} = \mu_N \sqrt{\frac{3}{16\pi}} \{(\gamma_n + \gamma_p) \boldsymbol{\sigma} + \boldsymbol{l} + [(1 - 2\xi_s)(\gamma_n - \gamma_p) \boldsymbol{\sigma} - (1 - 2\xi_l) \boldsymbol{l}] \tau_3\}, \quad (16)$$

where \boldsymbol{l} is the single-particle operator of the angular momentum, $\boldsymbol{\sigma}$ and τ_3 are the spin and isospin Pauli matrices, respectively (with positive eigenvalue of τ_3 for the neutrons), $\mu_N = e\hbar/2m_p c$ is the nuclear magneton, $\gamma_p = 2.793$ and $\gamma_n = -1.913$ are the spin gyromagnetic ratios, ξ_s and ξ_l are renormalization constants. Nonzero ξ_s and ξ_l correspond to an effective operator \mathcal{Q} . However, in the present calculations we used $\xi_l = 0$. Thus, the reduced probability of the $M1$ excitations $B(M1)$ is defined as $|\langle Z^n | \mathcal{Q} \rangle|^2$ in the RPA and as $|\langle z^\nu | \mathcal{Q} \rangle|^2$ in the RenTBA.

The Skyrme EDF with the basis parametrizations SKXm [33] and SV-bas [34] was used both in RPA and RenTBA.

TABLE I. Nuclear matter parameters: effective mass m^*/m , incompressibility K_∞ , Thomas-Reiche-Kuhn sum rule enhancement factor κ_{TRK} , and symmetry energy a_{sym} for two Skyrme-EDF parametrizations: SKXm [33] and SV-bas [34].

EDF	m^*/m	K_∞ (MeV)	κ_{TRK}	a_{sym} (MeV)
SKXm	0.97	238	0.34	31
SV-bas	0.90	233	0.40	30

The nuclear matter parameters for these parametrizations are listed in Table I.

There are four experimental characteristics of the $M1$ excitations in ^{208}Pb which serve as a benchmark in our calculations: energy and excitation probability of the isoscalar 1_1^+ state ($E_1 = 5.84$ MeV with $B_1(M1) = 2.0 \mu_N^2$, see Ref. [35]) and mean energy $E_2 = m_1/m_0$ and summed strength $B_2(M1) = m_0$ of the isovector $M1$ resonance computed from the moments $m_k = \sum_\nu B_\nu(M1) \omega_\nu^k$ summed in the interval 6.6–8.1 MeV ($E_2 = 7.4$ MeV with $B_2(M1) = 15.3 \mu_N^2$). The latter two quantities have been deduced by combining the data from Refs. [35,36].

In Table II, we show the results of the calculations of the $M1$ excitations in ^{208}Pb obtained within the self-consistent RPA and RenTBA using the Skyrme-EDF parametrizations SKXm and SV-bas. The value of the renormalization constant $\xi_s = 0.1$ adopted in Refs. [3,8] was used in the $M1$ operator Eq. (16). The set of the phonons in the RenTBA after the renormalization procedure with the condition Eq. (14) included 120 electric and 88 magnetic phonons for the parametrization SKXm and 120 electric and 115 magnetic phonons for the parametrization SV-bas. In all the cases, the calculated energies E_1 are too low and the probabilities $B_1(M1)$ are too large as compared with the data. In particular, $B_1(M1)_{\text{RPA}}$ for the SV-bas set is greater than $B_1(M1)_{\text{exp}}$ by a factor of 2.8. The mean energies E_2 and the summed strengths $B_2(M1)$ of the isovector $M1$ resonance are greater than the experimental values in the RPA and are less in the RenTBA. These examples demonstrate (see also the RPA results presented in Ref. [24]) that the self-consistent calculations based on the standard Skyrme-EDF parametrizations fail to give a

TABLE II. Energy E_1 and excitation probability $B_1(M1)$ of the isoscalar 1_1^+ state and the mean energy E_2 and the summed strength $B_2(M1)$ of the isovector $M1$ resonance in ^{208}Pb calculated within the self-consistent RPA and RenTBA with two Skyrme-EDF parametrizations: SKXm [33] and SV-bas [34]. The experimental data are taken from Refs. [35,36].

EDF	Model	E_1 (MeV)	$B_1(M1)$ (μ_N^2)	E_2 (MeV)	$B_2(M1)$ (μ_N^2)
SKXm	RPA	5.29	3.6	7.60	19.6
SKXm	RenTBA	4.81	3.3	6.77	14.9
SV-bas	RPA	5.66	5.6	7.95	17.8
SV-bas	RenTBA	5.02	4.7	6.90	13.1
Experiment		5.84	2.0	7.39	15.3

TABLE III. Parameters x_W , W_0 , g , and g' of the modified Skyrme EDFs determined on the basis of the parametrizations SKXm [33] and SV-bas [34]. The Landau-Migdal parameters g and g' are normalized to $C_N = 300 \text{ MeV} \cdot \text{fm}^3$. The renormalization constants ξ_s of the field operator of the $M1$ excitations corresponding to the each parametrization are shown in the last column. The parameters of the original sets are shown in the last two lines [with $g = G_0^{(300)}$ and $g' = G_0'^{(300)}$ where $G_0^{(300)}$ and $G_0'^{(300)}$ are the standard Landau-Migdal parameters (see, e.g., Ref. [24]) normalized to $C_N = 300 \text{ MeV} \cdot \text{fm}^3$].

EDF	x_W	W_0 ($\text{MeV} \cdot \text{fm}^5$)	g	g'	ξ_s
SKXm _{-0.54}	-0.54	226.0	-0.078	0.430	0.156
SV-bas _{-0.50}	-0.50	213.0	-0.028	0.516	0.156
SKXm _{-0.49}	-0.49	218.5	0.108	0.930	0.085
SKXm' _{-0.49}	-0.49	218.5	0.108	0.900	0.085
SKXm'' _{-0.49}	-0.49	218.5	-0.067	0.435	0.151
SV-bas _{-0.44}	-0.44	204.7	0.177	1.030	0.085
SV-bas' _{-0.44}	-0.44	204.7	0.177	1.460	0.085
SKXm	0	155.9	-0.154	0.543	
SV-bas	0.55	124.6	0.000	0.563	

quantitative description of the basic experimental characteristics of the low-energy $M1$ excitations in ^{208}Pb .

To reproduce the wanted key characteristics, we use the re-tuning strategy developed in Ref. [24]: The spin-related EDF parameters W_0 (spin-orbit strength), x_W (proton-neutron balance of the spin-orbit term), g (Landau parameter for isoscalar spin mode), and g' (Landau parameter for isovector spin mode) were refitted while the remaining spin-related parameters of the functional were switched off. The values of all other parameters of the functional were kept at the values of the original parametrizations. The form of the EDF containing all the parameters mentioned above is given in Ref. [24]. The spin-orbit parameters x_W and W_0 were refitted to reproduce the experimental value of $B_1(M1)$. The parameters g and g' enter the terms of the modified Skyrme EDF which yield the term V^s of the residual interaction V having the form of the Landau-Migdal ansatz

$$V^s = C_N (g \boldsymbol{\sigma} \cdot \boldsymbol{\sigma}' + g' \boldsymbol{\sigma} \cdot \boldsymbol{\sigma}' \boldsymbol{\tau} \cdot \boldsymbol{\tau}'), \quad (17)$$

where C_N is the normalization constant. These parameters allow us to change the calculated energies of the isoscalar and isovector 1^+ states while ground-state properties and natural parity modes remain basically unaffected.

Note that the parameter x_W was introduced in Refs. [37,38] (with the use of slightly different notations in Ref. [37]) to regulate the isospin dependence of the spin-orbit potential. In most parametrizations of the Skyrme EDF, a value $x_W \geq 0$ is used (see, e.g., last two lines of Table III). In particular, $x_W = 1$ (frequently used implicitly) corresponds to the EDF deduced from a two-body zero-range spin-orbit interaction. However, all these choices of x_W deliver for $B_1(M1)$ in ^{208}Pb calculated within the fully self-consistent RPA a value which is much larger than the experimental $B_1(M1)_{\text{exp}} = 2.0 \mu_N^2$ (see, e.g., Table II). For instance, $B_1(M1)_{\text{RPA}} \approx 10 B_1(M1)_{\text{exp}}$ for the SLy5 set [39] even with the use of the effective $M1$ operator (16). In Ref. [24] we have shown that one should

use negative values of x_W to decrease the calculated $B_1(M1)$ up to $B_1(M1)_{\text{exp}}$. The value of the parameter W_0 should be correspondingly increased because from the set of the refitted parameters x_W , W_0 , g , and g' , only the isoscalar combination of the spin-orbit parameters $C_0^{\text{VJ}} = -\frac{1}{4}(2 + x_W)W_0$ has an impact on the ground-state characteristics of spherical nuclei (see [24] for more details). This combination remains approximately unchanged in our refitting procedure, so the quality of the description of the ground-state properties with the use of the original and modified parametrizations of the Skyrme EDF is approximately the same.

IV. THE MAIN RESULTS FOR THE $M1$ RESONANCE IN ^{208}Pb

The parametrizations obtained from the refitting procedure described above are SKXm_{-0.54} and SV-bas_{-0.50} for the RPA and SKXm_{-0.49} and SV-bas_{-0.44} for the RenTBA (here and in the following the numerical subindex of the modified parametrization indicates the value of the parameter x_W). All four experimental characteristics of the $M1$ excitations in ^{208}Pb listed in the last line of Table II are reproduced in the RPA or RenTBA calculations based on these parametrizations. The set of phonons in the RenTBA included 123 electric and 83 magnetic phonons for the parametrization SKXm_{-0.49} and 121 electric and 85 magnetic phonons for the parametrization SV-bas_{-0.44}. The values of the refitted parameters are shown in Table III together with several sets discussed in Sec. VI. In addition, we used the renormalization constant ξ_s in the field operator of the $M1$ excitations Eq. (16) to fit the isovector $M1$ strength. The values of this constant for RPA and RenTBA are also shown in Table III.

The obtained values of the isoscalar parameter g for all modified parametrizations from Table III, except for SV-bas_{-0.44} and SV-bas'_{-0.44}, lie in the range $g \approx \pm 0.1$ coinciding with the range of the values of this parameter adopted in the non-self-consistent TFFS (see, e.g., Refs. [3,8,15–18,40]). The relatively large value $g = 0.177$ for the sets SV-bas_{-0.44} and SV-bas'_{-0.44} is explained by the combined effect of decreasing the spin-orbit parameter x_W and including the particle-phonon coupling in the RenTBA which is different for the SV-bas and SKXm parametrizations. The values of the isovector parameter g' for the RenTBA parametrizations SKXm_{-0.49} and SV-bas_{-0.44} are close to 1 that also is in agreement with the TFFS results.

Most of the calculations presented below have been performed within the discrete versions of RPA and RenTBA that means that the model equations are solved in a discrete basis representation using box boundary conditions. It is convenient to present these results as well as the experimental data in the form of a smooth strength functions $S(E)$ obtained by folding the discrete spectra with a Lorentzian of half-width Δ :

$$S(E) = \frac{\Delta}{\pi} \sum_v \frac{\text{sgn}(\omega_v) B_v(M1)}{(E - \omega_v)^2 + \Delta^2}. \quad (18)$$

The results for the modified SKXm parametrizations SKXm_{-0.49} (RenTBA) and SKXm_{-0.54} (RPA) obtained with folding parameter $\Delta = 20 \text{ keV}$ are shown in the upper panel of

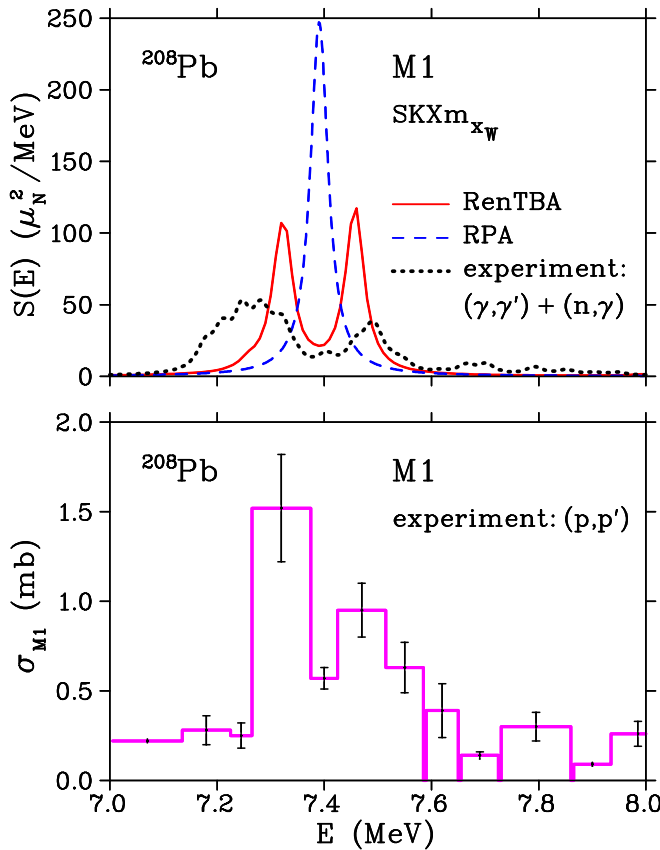


FIG. 1. Upper panel: strength distributions of the $M1$ excitations in ^{208}Pb calculated within the RenTBA with parametrization SKXm $_{-0.49}$ (red solid line) and within the RPA with parametrization SKXm $_{-0.54}$ (blue dashed line). The black dotted line represents the strength function Eq. (18) obtained from the experimental data [35,36]. The smearing parameter $\Delta = 20$ keV was used. See text for more details. Lower panel: the partial $M1$ cross section σ_{M1} of the $^{208}\text{Pb}(p, p')$ reaction from Ref. [41].

Fig. 1. The experimental spectra were taken from Refs. [35], $^{208}\text{Pb}(\gamma, \gamma')$ reaction, data below the neutron separation energy $S(n) = 7.37$ MeV, and Ref. [36], $^{207}\text{Pb}(n, \gamma)$ reaction, data above $S(n)$.

The RenTBA, in contrast to the RPA, reproduces the experimental splitting of the $M1$ resonance into two components separated by a dip near 7.4 MeV. The quantitative characteristics of this splitting are given in Table IV in comparison with the experimental data. The experimental summed $M1$ strength in the energy interval below the neutron threshold $\sum B(M1)_{<}$ is greater than the strength above the threshold $\sum B(M1)_{>}$ by about 50%, while the respective theoretical values are approximately equal to each other. Nevertheless, the total theoretical summed $M1$ strength in the interval 6.6–8.1 MeV is equal to the experimental one according to the conditions of construction of our modified parametrizations. The absolute values of the calculated mean energies $\bar{E}_{<}$ and $\bar{E}_{>}$ are close to the experimental values, however the differences $\Delta\bar{E} = \bar{E}_{>} - \bar{E}_{<}$ are different: the theoretical value $\Delta\bar{E}_{\text{theor}} = 0.14$ MeV is less than the experimental one $\Delta\bar{E}_{\text{exp}} = 0.31$ MeV by a factor of two. To estimate the frag-

TABLE IV. The summed strengths $\sum B(M1)$ and the mean energies \bar{E} of the $M1$ excitations calculated within the RenTBA with parametrization SKXm $_{-0.49}$ in two energy intervals. The last column contains the Gaussian width Γ of the $M1$ strength distribution calculated in the interval 6.6–8.1 MeV. The experimental data are taken from Refs. [35,36].

	6.60–7.37 MeV		7.37–8.10 MeV		Γ (MeV)
	$\sum B(M1)_{<}$ (μ_N^2)	$\bar{E}_{<}$ (MeV)	$\sum B(M1)_{>}$ (μ_N^2)	$\bar{E}_{>}$ (MeV)	
Theory	7.6	7.32	7.8	7.46	0.20
Experiment	9.2	7.26	6.2	7.57	0.44

mentation of the $M1$ resonance we have also calculated the equivalent Gaussian width Γ in the interval 6.6–8.1 MeV both for the experimental and for the theoretical strength distributions. The results presented in last column of Table IV show that the total width of the resonance is still underestimated.

The existence of the dip near the neutron separation energy in the experimental $M1$ strength distribution of ^{208}Pb is generally an uncertain point because the reliability of the experimental data [35,36] goes down in this region. To some extent, the possible existence of this dip is supported by the more recent data of the $^{208}\text{Pb}(p, p')$ experiment [41]. The partial $M1$ cross section σ_{M1} of this reaction is shown on the lower panel of Fig. 1. The dip in energy dependence of σ_{M1} near 7.4 MeV exists though it is less pronounced than for the strength function obtained from the data [35,36]. Note, however, the following: First, the direct comparison of the $M1$ strength functions $S(E)$ and the cross section $\sigma_{M1}(E)$ is hindered by the fact that they are determined by the different reaction mechanisms. The distribution of the $B(M1)$ values can be obtained from the cross section of the (p, p') reaction only within the framework of some model assumptions; see, e.g., Ref. [42]. Second, the dip near 7.4 MeV is absent in the distribution of $dB(M1)/dE$ deduced in Ref. [42] from the data of Ref. [41] and shown in Fig. 3(b) of Ref. [42]. But this fact can be explained by the different (and quite large) widths of the used energy bins that corresponds to the large and energy-dependent values of the smearing parameter Δ of the strength function Eq. (18).

V. THE FINE STRUCTURE OF THE $M1$ RESONANCE AND THE IMPACT OF THE SINGLE-PARTICLE CONTINUUM

To show the fine structure of the theoretical and experimental strength distributions and to study the role of the single-particle continuum (which in principle can manifest itself above the neutron separation energy), we have calculated the $M1$ strength functions in ^{208}Pb within the continuum RenTBA with $\Delta = 1$ and 0.1 keV. The single-particle continuum was included within the response function formalism according to the method developed in Ref. [31]. In this approach the strength function $S(E)$ is expressed through the response function, and the right-hand side of Eq. (18) is supplemented with the contribution of the continuum part of the spectrum. The parametrizations SKXm $_{-0.49}$ and SV-bas $_{-0.44}$

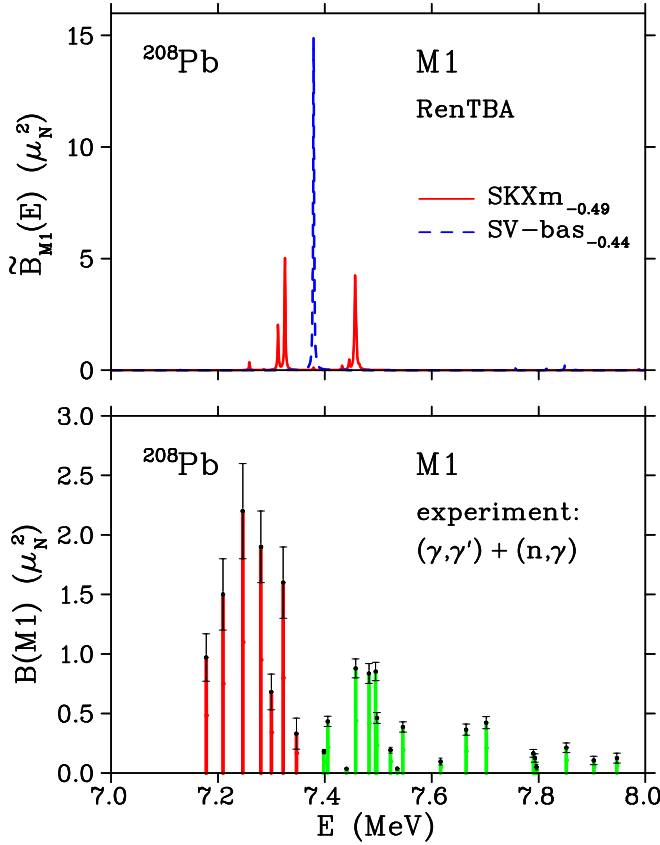


FIG. 2. Upper panel: strength distributions of the $M1$ excitations in ^{208}Pb calculated within the RenTBA with parametrizations SKXm $_{-0.49}$ (red solid line) and SV-bas $_{-0.44}$ (blue dashed line). The smearing parameter $\Delta = 1$ keV was used. See text for more details. Lower panel: experimental distribution of the excitation probabilities $B(M1)$ in ^{208}Pb in the interval 7–8 MeV from Refs. [35] [$^{208}\text{Pb}(\gamma, \gamma')$ reaction, red vertical lines] and [36] [$^{207}\text{Pb}(n, \gamma)$ reaction, green vertical lines]. The error bars are indicated by the black lines.

(the latter is discussed in more detail in Sec. VI) were used. The results for $\Delta = 1$ keV are shown on the upper panel of Fig. 2 in terms of the function $\tilde{B}_{M1}(E)$ defined as

$$\tilde{B}_{M1}(E) = \pi \Delta S(E). \quad (19)$$

Here we use this function because, as follows from Eq. (18),

$$B_v(M1) = \lim_{\Delta \rightarrow +0} \tilde{B}_{M1}(\omega_v). \quad (20)$$

So, if Δ is small, then the peak values of the function $\tilde{B}_{M1}(E)$ are close to the excitation probabilities at the peak energies. Note that Eq. (20) makes sense only for the states of the discrete spectrum. However, if Δ is greater than the escape width of the quasidecrete state in the continuum, then the peak value of the function $\tilde{B}_{M1}(E)$ allows us to estimate the integrated strength of the single resonance.

In the RenTBA calculation with the SKXm $_{-0.49}$ set and $\Delta = 1$ keV, the fragmentation of the two main peaks shown in Fig. 1 for the strength distributions with $\Delta = 20$ keV is very small. This picture does not match the detailed fragmentation structure of the experimental distribution composed from data

of Refs. [35,36] and shown on the lower panel of Fig. 2. The $M1$ strength in the interval 7–8 MeV obtained in the RenTBA with the parametrization SV-bas $_{-0.44}$ is concentrated in one state without visible fragmentation, as in the case of the RPA.

The lack of fragmentation in the presented RenTBA calculations can be explained by the limited (though extended as compared to the RPA) kinds of the correlations included in the model. There are two natural generalizations of the RenTBA which enable one to include the additional correlations. First is a model taking into account the so-called ground-state correlations beyond the RPA. In Refs. [17,18], it was shown that the inclusion of the correlations of this type increases the fragmentation of the $M1$ resonance in ^{208}Pb . The second generalization is the replacement of the intermediate $1p1h \otimes$ phonon configurations by two-phonon configurations according to the scheme suggested in Ref. [43] and in analogy with the first versions of the quasiparticle-phonon model [44]. Note that the relative importance of these additional correlations is increased at low energies due to the low level densities as compared to higher energies.

To analyze the effect of the single-particle continuum, we first note that the theoretical neutron separation energies are equal to 7.30 MeV for the parametrization SKXm $_{-0.49}$ and 7.64 MeV for the parametrization SV-bas $_{-0.44}$. So, the single peak of the RenTBA strength distribution for the SV-bas $_{-0.44}$ set shown on the upper panel of Fig. 2 (blue dashed line) is in the discrete spectrum, while the main strength of the distribution for the SKXm $_{-0.49}$ set (red solid line) lies in the continuum.

The effect of the continuum is determined by the values of the escape widths of the resonances. The full width at half maximum (FWHM) of the single peak of the strength distribution corresponding to the one or several overlapping resonances is formed by the escape and spreading widths and by the artificial width of 2Δ introduced by the smearing parameter. Thus, the FWHM can serve as an upper bound of the escape width. The distribution for the parametrization SKXm $_{-0.49}$ shown on the upper panel of Fig. 2 contains three main peaks with the energies 7.313 MeV, 7.325 MeV, and 7.457 MeV. These peaks correspond to four states of the discrete RenTBA spectrum with the energies 7.313 MeV, 7.326 MeV, 7.457 MeV, and 7.459 MeV which exhaust 92% of the summed strength of the $M1$ resonance in the interval 6.6–8.1 MeV. So, we can confine ourselves to analyzing the widths of only these peaks. The respective values of the FWHM are equal to 2.1 keV for the quasidecrete states with $E = 7.313$ MeV and 7.325 MeV and to 3.4 keV for the resonance with $E = 7.457$ MeV. The last FWHM value is appreciably greater than 2Δ . This is explained by the fact that the peak with $E = 7.457$ MeV is formed by two overlapping resonances which correspond to two states of the discrete spectrum mentioned above.

In the calculation with $\Delta = 0.1$ keV, the widths of the main peaks decrease. The values of the FWHM for the quasidecrete states with $E = 7.313$ and 7.325 MeV become less than 0.3 keV. The peak with $E = 7.457$ MeV is split into two peaks separated by the small interval of 2 keV and having the widths which are less than 1 keV. Thus, the escape widths of the main peaks of the distribution for the SKXm $_{-0.49}$ set are

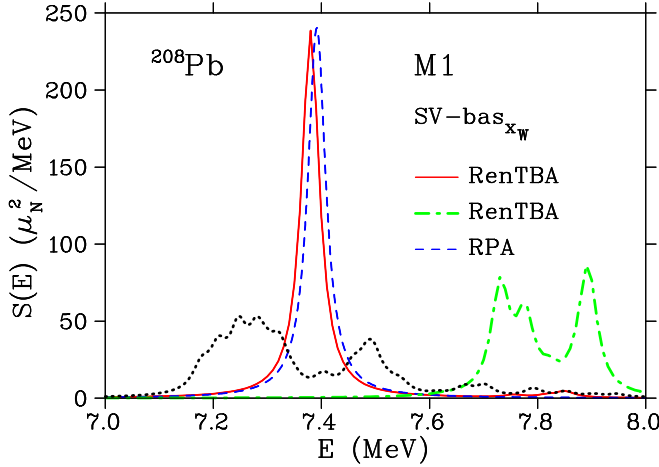


FIG. 3. Strength distributions of the $M1$ excitations in ^{208}Pb calculated within the RenTBA with parametrizations SV-bas $_{-0.44}$ (red solid line) and SV-bas' $_{-0.44}$ (green dashed-dotted line) and within the RPA with parametrization SV-bas $_{-0.50}$ (blue dashed line) in comparison with the experiment (black dotted line). The smearing parameter $\Delta = 20$ keV was used. See text for more details.

safely less than 1 keV. These results show that the inclusion of the single-particle continuum has no significant impact in the calculations with $\Delta = 20$ keV presented in the paper.

VI. THE PROBLEM OF THE FRAGMENTATION

The splitting of the isovector $M1$ resonance in ^{208}Pb into two main peaks obtained in RenTBA with the use of the parametrization SKXm $_{-0.49}$ is not a common result for the self-consistent calculations in our approach. In the typical case, if the EDF parameters g and g' are fitted to reproduce the experimental energy of the 1_1^+ state and the mean energy of the $M1$ resonance in ^{208}Pb , the fragmentation of the isovector $M1$ resonance is reduced to the quenching of the main peak without appreciable broadening. This quenching is compensated by decreasing the renormalization constant ξ_s , after which the forms of the RenTBA and RPA $M1$ distributions become close to each other. This is illustrated in Fig. 3 where we show results for the modified SV-bas parametrizations.

To clarify the problem, we note that the effects of the fragmentation of the RPA states in TBA and RenTBA are determined by the energy-dependent induced interaction $W(\omega)$, Eq. (8a). The fragmentation of the RPA state with the energy ω_{RPA} is strong if: (i) one or more energies Ω_c of the $1\text{p}1\text{h} \otimes$ phonon configurations in Eqs. (8) are close to the shifted energy $\tilde{\omega}_{\text{RPA}}$ (shifted due to the regular contribution of the remaining $1\text{p}1\text{h} \otimes$ phonon configurations) and (ii) the respective amplitudes $F_{ph}^{c(+)}$ are nonnegligible. In the case of ^{208}Pb , the isovector $M1$ strength in RPA is concentrated generally in one state with the energy $\omega_{\text{RPA}}(1_2^+)$ (the 1_1^+ RPA state is isoscalar), which is formed by two $1\text{p}1\text{h}$ configurations: $\pi(1h_{9/2} \otimes 1h_{11/2}^-)$ and $\nu(1i_{11/2} \otimes 1i_{13/2}^-)$. So, the ph indices of the amplitudes $F_{ph}^{c(+)}$ producing appreciable fragmentation of the 1_2^+ RPA state should be one of these two combinations. Under this condition and according to the selection rules for

TABLE V. The values of the particle-hole energies $\varepsilon_{ph}^\pi = \varepsilon_p^\pi(1h_{9/2}) - \varepsilon_h^\pi(3s_{1/2})$, the energies of 5_1^- phonon, and their sums Ω_c^{min} , Eqs. (21), in the RenTBA for the parametrizations SKXm $_{-0.49}$ and SV-bas $_{-0.44}$. The experimental values are given in the last line.

EDF	ε_{ph}^π (MeV)	$\omega(5_1^-)$ (MeV)	Ω_c^{min} (MeV)
SKXm $_{-0.49}$	4.14	3.24	7.38
SV-bas $_{-0.44}$	4.27	3.55	7.82
Experiment	4.21	3.20	7.41

the $M1$ excitations, the minimum value of Ω_c in ^{208}Pb is determined by the configuration $c = \{\pi(1h_{9/2} \otimes 3s_{1/2}^-) \otimes 5_1^-\}$, that is

$$\Omega_c^{\text{min}} = \varepsilon_{ph}^\pi + \omega(5_1^-), \quad (21a)$$

where

$$\varepsilon_{ph}^\pi = \varepsilon_p^\pi(1h_{9/2}) - \varepsilon_h^\pi(3s_{1/2}). \quad (21b)$$

It turns out that, for most Skyrme EDF parametrizations, the value of Ω_c^{min} is substantially greater than the mean energy of the isovector $M1$ resonance in ^{208}Pb , that is $\Omega_c^{\text{min}} > 7.4$ MeV. Thus, if the parameters of the EDF are fitted to reproduce this mean energy, then the fragmentation of the isovector $M1$ resonance is reduced to its quenching as mentioned above. The parametrization SKXm $_{-0.49}$ is an exception because the value of $\omega_{\text{RenTBA}}(5_1^-)$ comes close the experimental value which, in turn, yields an Ω_c^{min} close to 7.4 MeV. This is shown in Table V in comparison with the case of the SV-bas $_{-0.44}$ parametrization.

Note that the splitting of the isovector $M1$ resonance shown in Fig. 1 is achieved only in the RenTBA. In conventional TBA, the energies of the phonons in Eqs. (8) are calculated within the RPA. In the case of the parametrization SKXm $_{-0.49}$, the energy $\omega_{\text{RPA}}(5_1^-) = 3.64$ MeV that increases the energy Ω_c^{min} and leads to the RPA-like result in the TBA similar to what is shown in Fig. 3 by the red solid line.

On the other hand, the fragmentation of the isovector $M1$ resonance in ^{208}Pb in itself can be obtained also in the case $\Omega_c^{\text{min}} > 7.4$ MeV if the isovector $M1$ strength is shifted to higher energies by increasing the EDF parameter g' . This is shown in Fig. 3 for the parametrization SV-bas' $_{-0.44}$ which is constructed from the set SV-bas $_{-0.44}$ by changing the parameter g' from 1.03 for SV-bas $_{-0.44}$ to 1.46 for SV-bas' $_{-0.44}$ (however, the set of the phonons in this illustrative RenTBA calculation for SV-bas' $_{-0.44}$ was the same as for SV-bas $_{-0.44}$). Thus, it seems that the simultaneous description of the mean energy of the isovector $M1$ resonance in ^{208}Pb together with the fragmentation of this resonance in the self-consistent calculation is possible only in rare circumstances as, e.g., in case of the parametrization SKXm $_{-0.49}$.

Note that the fragmentation of the isovector $M1$ resonance in ^{208}Pb was obtained in the early calculations within the shell model in the $1\text{p}1\text{h} + 2\text{p}2\text{h}$ space [10] and within the models based on the TFFS [9] including the particle-phonon interaction on top of the RPA (see, e.g., Refs. [11,12,15,17,18]). This result is explained by two reasons. First, the mean

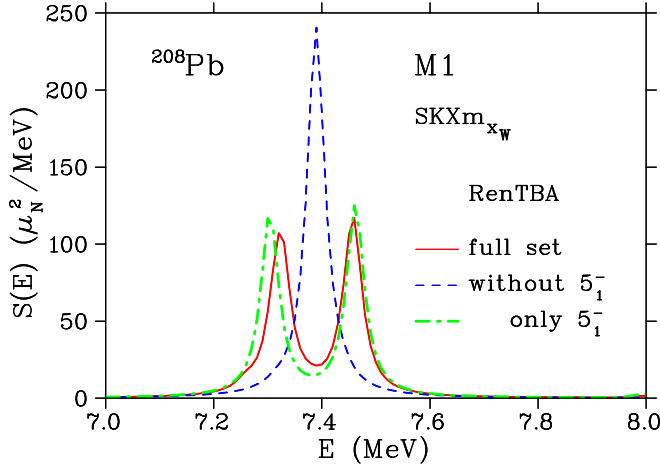


FIG. 4. Strength distributions of the $M1$ excitations in ^{208}Pb calculated within the RenTBA with the full set of the phonons and with parametrization $\text{SKXm}_{-0.49}$ (red solid line), with the set of all the phonons except for the 5_1^- phonon and with parametrization $\text{SKXm}'_{-0.49}$ (blue dashed line) and with the set of the phonons including only the 5_1^- phonon and with parametrization $\text{SKXm}''_{-0.49}$ (green dashed-dotted line). The smearing parameter $\Delta = 20$ keV was used. See text for more details.

energy of the isovector $M1$ resonance in these calculations was above the experimental value. The shift to higher energies increases the spreading of the $M1$ strength as was noted in Ref. [10] and is demonstrated in Fig. 3. Second, the phonon energies in the calculations of Refs. [12,15,17,18] were fitted to their experimental values that brings the value of Ω_c^{min} closer to the mean energy of the isovector $M1$ resonance, see Table V.

To demonstrate the role of the intermediate $1p1h \otimes$ phonon configuration $\pi(1h_{9/2} \otimes 3s_{1/2}^-) \otimes 5_1^-$ in the effect of the fragmentation under discussion we show in Fig. 4 the results of three RenTBA calculations with the use of parametrizations $\text{SKXm}_{-0.49}$, $\text{SKXm}'_{-0.49}$, and $\text{SKXm}''_{-0.49}$ (see Table III). The RenTBA calculation with the parametrization $\text{SKXm}_{-0.49}$ coincides with the one shown in Fig. 1. In the calculation with $\text{SKXm}'_{-0.49}$, the 5_1^- phonon was excluded and the EDF parameter g' was slightly changed to fit the mean energy of the isovector $M1$ resonance to the experiment. The calculation with $\text{SKXm}''_{-0.49}$ represents the opposite case: only the 5_1^- phonon was included in the phonon basis of the RenTBA and the EDF parameters g and g' were changed to fit the energy of the 1_1^+ state and the mean energy of the isovector $M1$ resonance to the experiment. The renormalization constant ξ_s was also changed to compensate the reduced quenching of the $M1$ strength. However, the characteristics of the same phonons (energies, etc.) were the same in all three calculations. These results show that the splitting of the isovector $M1$ resonance in ^{208}Pb is determined in the considered model practically exclusively by the configuration $\pi(1h_{9/2} \otimes 3s_{1/2}^-) \otimes 5_1^-$. The other $1p1h \otimes$ phonon configurations produce only the shift of the $M1$ resonance and the quenching of the $M1$ strength.

TABLE VI. The energies (in MeV) of the first excited states of the natural parity in ^{208}Pb calculated within the RenTBA and the RPA with the use of the modified Skyrme EDFs $\text{SKXm}_{-0.49}$ and $\text{SV-bas}_{-0.44}$. The experimental data are taken from Ref. [45].

L^π	$\text{SKXm}_{-0.49}$		$\text{SV-bas}_{-0.44}$		Experiment
	RenTBA	RPA	RenTBA	RPA	
2_1^+	4.01	4.45	4.00	4.42	4.09
3_1^-	2.69	2.91	2.88	3.10	2.61
4_1^+	4.29	4.81	4.30	4.80	4.32
5_1^-	3.19	3.64	3.49	3.93	3.20
6_1^+	4.43	5.02	4.53	5.13	4.42

VII. RESULTS FOR THE LOW-ENERGY ELECTRIC EXCITATIONS IN ^{208}Pb

In Sec. VI, we have shown that the RenTBA using the modified Skyrme EDF $\text{SKXm}_{-0.49}$ gives an energy of the first 5_1^- state in ^{208}Pb close to its experimental value. Here we consider the results of the RenTBA and RPA calculations for the first excited states of natural parity in ^{208}Pb with the multipolarity L from 2 to 6 both for the $\text{SKXm}_{-0.49}$ and the $\text{SV-bas}_{-0.44}$ parametrizations. The results are presented in Tables VI and VII. Note that the RenTBA results have been obtained without use of the diagonal approximation which is used in the model only for the phonons entering the intermediate $1p1h \otimes$ phonon configurations. It explains the small difference between the energies of the 5_1^- state listed in Tables V (where the diagonal approximation is used) and VI.

The RenTBA energies calculated with the parametrization $\text{SKXm}_{-0.49}$ agree fairly well with the experiment. The deviations for $\text{SV-bas}_{-0.44}$ are slightly greater (except for the 4_1^+ state). The RPA gives too large energies for both parametrizations. The energy shift $\omega(\text{RPA}) - \omega(\text{RenTBA})$ is between 0.2 MeV for the 3_1^- state and 0.6 MeV for the 6_1^+ state.

The situation is the opposite for the excitation probabilities shown in Table VII. The RPA results are closer to the experiment as compared to the RenTBA results (and are in a good agreement with the experiment for 2_1^+ , 3_1^- , and 4_1^+ states). The decrease of the $B(EL)$ values in RenTBA is caused by the quenching as in the case of the $M1$ excitations.

By construction, the modified parametrizations $\text{SKXm}_{-0.49}$ and $\text{SV-bas}_{-0.44}$ describe the nuclear

TABLE VII. The same as in Table VI but for the excitation probabilities $B(EL)$ (in units of $e^2\text{fm}^{2L}$).

L^π	$\text{SKXm}_{-0.49}$		$\text{SV-bas}_{-0.44}$		Experiment
	RenTBA	RPA	RenTBA	RPA	
2_1^+	2.6×10^3	3.2×10^3	2.5×10^3	3.0×10^3	3.2×10^3
3_1^-	5.6×10^5	6.4×10^5	5.8×10^5	6.4×10^5	6.1×10^5
4_1^+	1.1×10^7	1.5×10^7	9.6×10^6	1.3×10^7	1.6×10^7
5_1^-	1.9×10^8	2.9×10^8	2.3×10^8	3.6×10^8	4.5×10^8
6_1^+	2.6×10^{10}	3.6×10^{10}	1.4×10^{10}	2.2×10^{10}	6.7×10^{10}

ground-state properties within the Skyrme EDF approach (with approximately the same accuracy as the original parametrizations SKXm and SV-bas) and reproduce the basic experimental characteristics of the $M1$ excitations in ^{208}Pb within the RenTBA. The results of this section show that the RenTBA with the use of these modified parametrizations is applicable also to the description of the low-energy electric excitations in this nucleus.

VIII. CONCLUSIONS

The present paper is a continuation of our recent work [24] in which we investigated the low-energy $M1$ excitations in ^{208}Pb within the self-consistent RPA based on the Skyrme energy-density functionals (EDF). Here we use the extended self-consistent model including the particle-phonon coupling within the renormalized time blocking approximation (RenTBA, [25]). As in the case of the self-consistent RPA, the description of the basic experimental characteristics of the $M1$ excitations in ^{208}Pb (energy and strength of the 1_1^+ state as well as mean energy and summed strength of the isovector $M1$ resonance) requires refitting some of the

spin-related parameters of the Skyrme EDF within the self-consistent RenTBA. We have determined several sets of these parameters from this condition. It has been shown that the observed fragmentation of the isovector $M1$ resonance in ^{208}Pb which is absent in all the RPA calculations can be to a certain extent described within the self-consistent RenTBA. However, this description is not fully quantitative and is attained only in some cases of the modified functionals of the Skyrme type. We have found that the necessary condition to obtain this fragmentation in our model is that the energy of the intermediate $1p1h \otimes$ phonon configuration $\pi(1h_{9/2} \otimes 3s_{1/2}^-) \otimes 5_1^-$ comes close to the mean energy of the isovector $M1$ resonance in ^{208}Pb , that is achieved if the energy of 5_1^- phonon comes close to the experimental excitation energy of the 5_1^- state in ^{208}Pb . We have also shown that the modified parametrizations of the Skyrme EDF presented in the paper can be used in the description of the low-energy electric excitations within the RenTBA.

ACKNOWLEDGMENTS

V.T. is grateful to Prof. V. Yu. Ponomarev for discussions. Research was carried out using computational resources provided by Resource Center “Computer Center of SPbU.”

-
- [1] M. Bender, P.-H. Heenen, and P.-G. Reinhard, *Rev. Mod. Phys.* **75**, 121 (2003).
 - [2] R. M. Laszewski, R. Alarcon, D. S. Dale, and S. D. Hoblit, *Phys. Rev. Lett.* **61**, 1710 (1988).
 - [3] S. Kamenrzhiev, J. Speth, and G. Tertychny, *Phys. Rep.* **393**, 1 (2004).
 - [4] J. D. Vergados, *Phys. Lett. B* **36**, 12 (1971).
 - [5] P. Ring and J. Speth, *Phys. Lett. B* **44**, 477 (1973).
 - [6] V. N. Tkachev, I. N. Borzov, and S. P. Kamenrzhiev, *Sov. J. Nucl. Phys.* **24**, 373 (1976).
 - [7] J. Speth, V. Klemt, J. Wambach, and G. E. Brown, *Nucl. Phys. A* **343**, 382 (1980).
 - [8] I. N. Borzov, S. V. Tolokonnikov, and S. A. Fayans, *Sov. J. Nucl. Phys.* **40**, 732 (1984).
 - [9] A. B. Migdal, *Theory of Finite Fermi Systems and Application to Atomic Nuclei* (Wiley, New York, 1967).
 - [10] T.-S. H. Lee and S. Pittel, *Phys. Rev. C* **11**, 607 (1975).
 - [11] J. S. Dehesa, J. Speth, and A. Faessler, *Phys. Rev. Lett.* **38**, 208 (1977).
 - [12] S. P. Kamenrzhiev and V. N. Tkachev, *Phys. Lett. B* **142**, 225 (1984).
 - [13] D. Cha, B. Schwesinger, J. Wambach, and J. Speth, *Nucl. Phys. A* **430**, 321 (1984).
 - [14] D. T. Khoa, V. Y. Ponomarev, and A. I. Vdovin, Preprint JINR **E4-86-198** (1986).
 - [15] S. P. Kamenrzhiev and V. N. Tkachev, *Z. Phys. A* **334**, 19 (1989).
 - [16] V. I. Tselyaev, *Sov. J. Nucl. Phys.* **50**, 780 (1989).
 - [17] S. P. Kamenrzhiev and V. I. Tselyaev, *Bull. Acad. Sci. USSR, Phys. Ser.* **55**, 45 (1991).
 - [18] S. P. Kamenrzhiev, J. Speth, G. Tertychny, and J. Wambach, *Z. Phys. A* **346**, 253 (1993).
 - [19] L.-G. Cao, G. Colò, H. Sagawa, P. F. Bortignon, and L. Sciacchitano, *Phys. Rev. C* **80**, 064304 (2009).
 - [20] P. Vesely, J. Kvasil, V. O. Nesterenko, W. Kleinig, P.-G. Reinhard, and V. Y. Ponomarev, *Phys. Rev. C* **80**, 031302(R) (2009).
 - [21] V. O. Nesterenko, J. Kvasil, P. Vesely, W. Kleinig, P.-G. Reinhard, and V. Y. Ponomarev, *J. Phys. G: Nucl. Part. Phys.* **37**, 064034 (2010).
 - [22] L.-G. Cao, H. Sagawa, and G. Colò, *Phys. Rev. C* **83**, 034324 (2011).
 - [23] P. Wen, L.-G. Cao, J. Margueron, and H. Sagawa, *Phys. Rev. C* **89**, 044311 (2014).
 - [24] V. Tselyaev, N. Lyutorovich, J. Speth, P.-G. Reinhard, and D. Smirnov, *Phys. Rev. C* **99**, 064329 (2019).
 - [25] V. Tselyaev, N. Lyutorovich, J. Speth, and P.-G. Reinhard, *Phys. Rev. C* **97**, 044308 (2018).
 - [26] C. Toepffer and P.-G. Reinhard, *Ann. Phys. (NY)* **181**, 1 (1988).
 - [27] K. Gütter, P.-G. Reinhard, K. Wagner, and C. Toepffer, *Ann. Phys. (NY)* **225**, 339 (1993).
 - [28] V. I. Tselyaev, *Phys. Rev. C* **88**, 054301 (2013).
 - [29] N. Lyutorovich, V. Tselyaev, J. Speth, S. Krewald, F. Grümmer, and P.-G. Reinhard, *Phys. Lett. B* **749**, 292 (2015).
 - [30] N. Lyutorovich, V. Tselyaev, J. Speth, S. Krewald, and P.-G. Reinhard, *Phys. At. Nucl.* **79**, 868 (2016).
 - [31] V. Tselyaev, N. Lyutorovich, J. Speth, S. Krewald, and P.-G. Reinhard, *Phys. Rev. C* **94**, 034306 (2016).
 - [32] J. Speth, E. Werner, and W. Wild, *Phys. Rep.* **33**, 127 (1977).
 - [33] B. A. Brown, *Phys. Rev. C* **58**, 220 (1998).
 - [34] P. Klüpfel, P.-G. Reinhard, T. J. Bürvenich, and J. A. Maruhn, *Phys. Rev. C* **79**, 034310 (2009).
 - [35] T. Shizuma, T. Hayakawa, H. Ohgaki, H. Toyokawa, T. Komatsubara, N. Kikuzawa, A. Tamii, and H. Nakada, *Phys. Rev. C* **78**, 061303(R) (2008).
 - [36] R. Köhler, J. A. Wartena, H. Weigmann, L. Mewissen, F. Poortmans, J. P. Theobald, and S. Raman, *Phys. Rev. C* **35**, 1646 (1987).

- [37] P.-G. Reinhard and H. Flocard, *Nucl. Phys. A* **584**, 467 (1995).
- [38] M. M. Sharma, G. Lalazissis, J. König, and P. Ring, *Phys. Rev. Lett.* **74**, 3744 (1995).
- [39] E. Chabanat, P. Bonche, P. Haensel, J. Meyer, and R. Schaeffer, *Nucl. Phys. A* **635**, 231 (1998).
- [40] E. Migli, S. Drożdż, J. Speth, and J. Wambach, *Z. Phys. A* **340**, 111 (1991).
- [41] I. Poltoratska, P. von Neumann-Cosel, A. Tamii, T. Adachi, C. A. Bertulani, J. Carter, M. Dozono, H. Fujita, K. Fujita, Y. Fujita, K. Hatanaka, M. Itoh, T. Kawabata, Y. Kalmykov, A. M. Krumbholz, E. Litvinova, H. Matsubara, K. Nakanishi, R. Neveling, H. Okamura, H. J. Ong, B. Özel-Tashenov, V. Y. Ponomarev, A. Richter, B. Rubio, H. Sakaguchi, Y. Sakemi, Y. Sasamoto, Y. Shimbara, Y. Shimizu, F. D. Smit, T. Suzuki, Y. Tameshige, J. Wambach, M. Yosoi, and J. Zenihiro, *Phys. Rev. C* **85**, 041304(R) (2012).
- [42] J. Birkhan, H. Matsubara, P. von Neumann-Cosel, N. Pietralla, V. Y. Ponomarev, A. Richter, A. Tamii, and J. Wambach, *Phys. Rev. C* **93**, 041302(R) (2016).
- [43] V. I. Tselyaev, *Phys. Rev. C* **75**, 024306 (2007).
- [44] V. G. Soloviev, *Theory of Atomic Nuclei: Quasiparticles and Phonons* (Institute of Physics, Bristol and Philadelphia, 1992).
- [45] M. Martin, *Nucl. Data Sheets* **108**, 1583 (2007).